Heliyon 7 (2021) e08180

Contents lists available at ScienceDirect

Heliyon

journal homepage: www.cell.com/heliyon

Research article

Polyaniline nanofibers, a nanostructured conducting polymer for the remediation of Methyl orange dye from aqueous solutions in fixed-bed column studies

Mbongiseni Lungelo Dlamini [a], Madhumita Bhaumik [c], Kriveshini Pillay [a,*], Arjun Maity [a,b,**]

[a] Department of Applied Chemistry, University of Johannesburg, 2028, Doornfontein, Johannesburg, South Africa
[b] DST/CSIR National Centre for Nanostructured Materials, Council for Scientific and Industrial Research, 1-Meiring Naude Road, Pretoria, 0001, South Africa
[c] Department of Physics, University of South Africa, Johannesburg, 1710, South Africa

ARTICLE INFO

Keywords:
Polyaniline
Nanofibers
Methyl orange
Adsorption
Fixed-bed
Modeling

ABSTRACT

Polyaniline nanofibers (PANI NFs) were synthesized and employed as potential adsorbents in a continuous flow fixed-bed column adsorption study for an organic dye, Methyl Orange (MO) removal from water. These nanostructured adsorbents were characterized using ATR-FTIR, FE-SEM, HR-TEM, TGA, BET, XRD, XPS, and the Zetasizer. Morphological representations from SEM and TEM analyses showed that the fibers were nanosized with diameters lower than 80 nm and an interconnected network possessing a smooth surface. The S_{BET} of the PANI NFs was found to be 35.80 m^2/g. The impact of column design parameters for instance; influent concentration, flow rate, and bed mass was investigated using pH 4 influent MO solutions optimized through batch studies. The best influent concentration, bed length, and flow rate for this study were determined as 25 mg/L, 9 cm (6 g), and 3 mL/min, respectively. The column information was fitted in Thomas, Yoon-Nelson, and Bohart-Adams models. It appeared that the Thomas and Yoon-Nelson models described the data satisfactorily. The PANI NFs were able to treat 29.16 L of 25 mg/L MO solution at 9 cm bed length. A sulfate peak in a de-convoluted sulfur spectrum using XPS verified the successful adsorption of Methyl Orange.

1. Introduction

Discoloration is a good indicator of contamination. Significant amounts of contaminated colored effluents are generated as a result of the usage of chromophore-containing compounds, such as dyes or pigments from the textile, printing, paper, leather, cosmetics, and pharmaceutical industries [1, 2]. The toxic dyes contribute to the drastic increase of environmental pollution. Such dyes are highly toxic and non-biodegradable. As a result, they are extremely dangerous to people and other living species, posing a severe environmental threat [3, 4]. Although some dyes may be non-toxic and inert at the concentration at which they are discharged into the receiving water, they impart color in the water system, which may restrict light penetration and hence hinder photosynthesis in aquatic vegetation, adversely impacting both aquatic flora and fauna [1, 5]. This results in the disruption of food webs which ultimately affects the entire aquatic ecosystems. Synthetic dyes reign supreme among various synthetic azo dyes. A good example of an anionic azo dye that falls into this category is Methyl Orange (MO), which is found in the industrial effluents of textile industries [6]. The MO structure is represented in Figure 1, showing the azo bond (-N=N-) and the sulfonate group.

Environmental "eye-sores" due to discoloration and health problems are instigated by the discharge of such colourants into natural and living surroundings [7]. The persistence of these dyes in the environment can lead to health effects in living organisms, which include carcinogenic and mutagenic effects. It is therefore imperative that such colourants be eliminated from regular water bodies and supplies. In this sense, several physico-chemical technologies, such as coagulation/flocculation [8, 9], chemical oxidation [10, 11, 12, 13], ion exchange [14, 15, 16], membrane separation [17, 18], electrochemical techniques [19, 20],

* Corresponding author.
** Corresponding author.
E-mail addresses: kriveshinip@uj.ac.za (K. Pillay), maityarjun@gmail.com, AMaity@csir.co.za (A. Maity).

https://doi.org/10.1016/j.heliyon.2021.e08180
Received 17 May 2021; Received in revised form 7 August 2021; Accepted 11 October 2021

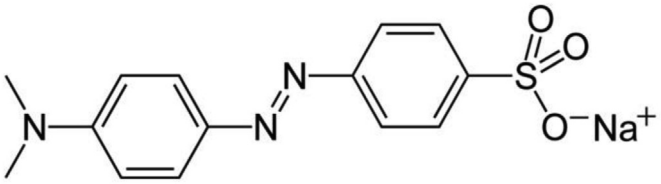

Figure 1. Chemical structure of Methyl orange.

adsorption [6, 21] and photo-catalysis [22, 23, 24, 25], have been explored in the remediation of dye-containing wastewaters. However, drawbacks such as low efficiency, high sludge generation, intensive energy requirements, and most importantly their high installation cost associated with membrane technology [18, 26] impede the application of such technologies for the remediation of MO. Adsorption has been identified as the most attractive and highly potent technique for remediation of most contaminants (including dyes) from water. This is due to its relatively simple operation, high adsorption efficiency, and the lack of production of secondary waste, which can cause further harm to the environment. This technique also offers the advantage of simple scaling from laboratory scale to field scale [2, 27, 28] and the availability of a vast array of adsorbents [21, 29].

Since cost has been a crucial factor in the applicability of water treatment systems, investigation attentiveness into the invention of alternative cost-effective sorbents has intensified in the recent years [20, 29]. To date, multiple natural and artificial sorbents have been employed for MO remediation from wastewater. These include polypyrrole nanofibers [28], activated carbon [30], modified coffee waste [31], chitosan hydrogel beads [32], magnetic iron oxide/carbon nanocomposite [33], amino-crosslinked hypromellose [34], bentonite and coffee grounds activated [34, 35], waste ash [36], populous tree leaves [37], manganese-rich synthetic mica [35], *etc*. However, all of these adsorbents were explored in batch adsorption mode, which is well acknowledged to provide insufficient information for scaling up [38, 39, 40]. Therefore, it is imperative to develop a new, highly efficient adsorbent, and investigate its behavior in continuous flow fixed-bed column adsorption studies. Column sorption try-outs are generally preferred in practical applications for continuous wastewater treatment as well as potential simulations of permeable reactive barriers for groundwater pollutant decontamination [41, 42]. This is due to the continuous concentration gradient which controls the extent of adsorption [39]. It also makes provision for better exploitation of the adsorbent capacity leading to improved water quality [43, 44].

Polyaniline (PANI), polypyrrole (PPy), and polythiophene (PTh) are three of the most conventional conducting electroactive polymers that have in the last two decades attracted a great deal of attention [45, 46, 47, 48, 49, 50, 51, 52, 53]. Quite a number of applications such as optical, electronics, and adsorption have employed these conducting polymers [54, 55, 56]. This is due to their easy and economical synthesis, good electrochemical and electrical properties [55, 57, 58]. Additionally, in the presence of oxygen and water, these conducting polymers exhibit high environmental stability [59, 60, 61]. PANI and PPy have been highly recommended for wastewater remediation. However, PANI stands out among the family of conjugated and conducting polymers, owing to its inherent properties associated with reversible acid/base doping/de-doping chemistry [52]. The characteristic positively charged nitrogen atoms on the polymeric backbone of PANI offer additional benefits, such as suitable adsorption sites for the elimination of anionic contaminants via electrostatic interactions. Recently, nanostructured PANI in the form of nanofibers, nano-spheres, *etc*. has generated much scientific interest. This is mainly due to the structural effect of nano-dimensional organic conductors with enhanced surface area which is characteristic of nanostructured materials [61].

A variety of fabrication approaches of PANI nanofibers (PANI NFs) have been reported. These include electrochemical synthesis, electrospinning [62, 63] and soft and hard templates [64], and many more. However, these methods are very complex and not very economical for industrial applications. Moreover, the preparation of pure PANI NFs also requires some additional steps. There are various simple ways to synthesize PANI NFs without using templates. One of these methods is the intrinsic formation of NFs when PANI polymerises [65, 66]. Such a simple method normally involves either rapid mixing chemical or interfacial polymerization. Usually, the aniline monomer and oxidizing agents are quickly mixed and there is no further addition of aniline monomers once the PANI NFs form. Another advantage which this technique offers is the lack of use of organic solvents or other assisting techniques [64, 67, 68].

Reports on the use of PANI NFs for the environmental remediation of organic and inorganic pollutants from wastewater are scarce. Thus, the focus of this study was to investigate the ability of PANI NFs, fabricated via a simple quick mixing polymerization procedure to adsorb MO dye from synthetic water through a fixed phase column adsorption study. The following objectives were set: (i) to synthesize polyaniline nanofibers and characterize the adsorbent, (ii) to evaluate the adsorption efficiency of the adsorbent for MO dye removal from synthetic water in fixed-bed adsorption mode, (iii) to examine the influence of process factors such as influent concentration, flow rate and bed length by means of a breakthrough curve, and (iv) to explore mathematical modeling of column data breakthrough to characterize the sorption processes in the fixed phase experiments.

2. Materials and methods

2.1. Reagents

The monomer aniline (ANI, 99%), an oxidizing agent iron (III) chloride ($FeCl_3$), hydrochloric acid (HCl), sodium hydroxide (NaOH) and methyl orange (MO) dye powder were of Sigma–Aldrich origin, USA. Aniline monomer first underwent purification by distillation under vacuum. Only analytical grade chemicals were used. The preparation of 1000 mg/L MO stock solution was performed and subsequently watered down to solutions of lower concentrations as required for the column studies.

2.2. Preparation of PANI nanofibers (PANI NFs)

A chemical oxidative polymerisation technique in which aniline monomers were quickly mixed with iron (III) chloride ($FeCl_3$) (oxidant) at room temperature was employed to prepare the PANI-NFs (Bhaumik et al., 2016; Bhaumik et al., 2015). This involved the dissolution of 6 g of $FeCl_3$ in distilled water (80 mL) in a 250 ml conical flask. To this solution, 0.8 mL of aniline monomer was introduced via syringe under adequate magnetic stirring. The continuous stirring is meant to create an even distribution between molecules of the oxidant and monomer prior to polymerization. This helps to prevent any further polyaniline development. The mixture was stirred continuously for 5 min and then left undisturbed for 2 days (48 h). This step allowed the polymerization reaction to proceed without stirring. The PANI NFs were obtained by filtration through a vacuum filter. The final product was then rinsed with deionised water to obtain a colourless filtrate. Subsequent washing with acetone was conducted to remove excess oligomers. Ultimately, the nanofibers were oven dried under vacuum set at 60 °C for 24 h.

2.3. Characterization of PANI NFs

An FTIR spectrum of polyaniline nanofibers was recorded on a Perkin–Elmer, USA attenuated total reflectance Fourier Transform Infrared (ATR-FTIR) Spectrum 100 spectrometer in the range 500–4000 cm^{-1}. To

investigate the surface and in-depth morphology of the PANI NFs, an Auriga Field Emission Scanning Electron Microscope (FE-SEM; Zeiss Auriga Cobra FIB, Germany) and a JEOL JEM-2100 High Resolution Transmission Electron Microscope (HR-TEM; JEOL, Japan) were used, respectively. High resolution TEM images were obtained on a high resolution-TEM instrument operated with a LaB6 filament at 200 kV. The TGA experiments were conducted in air at 50 mL/min flow rate with the instrument set at 10 °C/min heating rate on TGA Q500 (TA Instruments, USA). The BET surface area of the adsorbent was measured using a Micromeritics ASAP 2020 gas adsorption apparatus (USA). A PANalytical X'Pert PRO-diffractometer (PANalytical, The Netherlands) was employed for XRD measurements by means of CuKα radiation with 1.5505 Å wavelength and slits at 45 kV/30 mA for 2θ values ranging from 5° to 90°. Kratos Axis Ultra device with Al monochromatic X-ray source (1486.6 eV) was used for XPS analysis. The zeta potential of the adsorbent (PZC) was obtained from a Malvern Zeta-Sizer particle size measurement instrument of Malvern Ltd, UK origin.

2.4. Fixed-bed adsorption experiments

As described earlier, 1000 mg/L MO stock solutions were prepared and diluted as required for each experiment. Laboratory scale fixed-bed column adsorption experiments were conducted to determine the PANI NFs' efficiency in adsorptive removal of MO dye from synthetic wastewater. The PANI NFs were packed into an adsorption column which was composed of a perspex glass designed into a cylinder-shaped tube with the dimensions; 1.4 cm diameter and 30 cm length. The PANI-NFs were sandwiched between layers of glass wool and braced by non-reactive glass beads at both ends of the column as shown in Figure 2. The influent, MO solution, was adjusted to pH 4 which was optimized in batch studies. To prevent channeling inside the column and ensure homogeneous flow, a peristaltic pump was used to force the solution up the column tube. Prior to the adsorption process, the column contents were rinsed with deionized water to equilibrate the adsorbent particles. The temperature for all adsorption studies was fixed at ~25 °C (ambient temperature). For maintenance of constant flow during the experiment, the effluent solution was collected at periodic intervals in a measuring cylinder for a minute. This, therefore, helped to monitor the flow rate. Analysis for residual MO concentration was conducted on a Perkin Elmar Lambda UV-vis spectrophotometer at λ_{max} = 464 nm after the effluent was sampled at specific time intervals. As the effluent was collected, when its concentration approached equivalence, relative to inlet concentration, the column operation was terminated as this signified attainment of adsorbent saturation.

2.4.1. Breakthrough analysis

The term adsorption essentially infers adhesion of a substance termed adsorbate onto the surface of a material referred to as the adsorbent. In typical fixed-bed column systems, the adsorbent closer to the influent point tends to saturate first, since this is the point where maximum adsorption occurs. The adsorption zone will then progressively migrate up the adsorbent bed with time and eventually reaches the point of bed exit, which is called the breakthrough point. When the sorbate reaches the bed exit, the outlet adsorbate concentration will be almost equal to the inlet concentration [70].

The theory of breakthrough curves was applied in predicting the performance of the fixed-bed column [38, 39, 71]. Breakthrough curves provide a coherent indication of the breakthrough point and are therefore vital for column adsorption systems. For the MO column adsorption, the breakthrough point was set at 0.5%. This is basically the point in time when the collected MO concentration reached 0.5% of the influent concentration. The packed adsorbent (PANI NFs) was deemed saturated when the effluent MO concentration reached 85% of the inlet concentration [42]. The breakthrough curves are characterized by a plot of C_t/C_o versus time in h, where C_t/C_o represents the ratio of effluent concentration at time t to influent concentration. The effects of design parameters like bed mass, flow rate, and influent concentration were inspected.

The adsorption performance is directly associated with the processed bed volumes, (BV) at a fixed bed length afore attainment of breakthrough point [72]. The BV essentially quantifies the volume of water that can undergo treatment per unit volume of adsorbent bed, hence high BV signifies high performance [73]. Eq. (1) is used to calculate BV:

$$\mathrm{BV} = \frac{\text{volume of water treated at breakthrough point (L)}}{\text{volume of adsorbent bed (L)}} \quad (1)$$

Additionally, the rate of adsorbent exhaustion can be used to establish the frequency at which the adsorbent needs to be replaced. This can be calculated from Eq. (2) [72]:

$$\mathrm{AER} = \frac{\text{mass of adsorbent (g)}}{\text{volume of water treated (L)}} \quad (2)$$

In general, if AER is low, the bed performance is considered good.

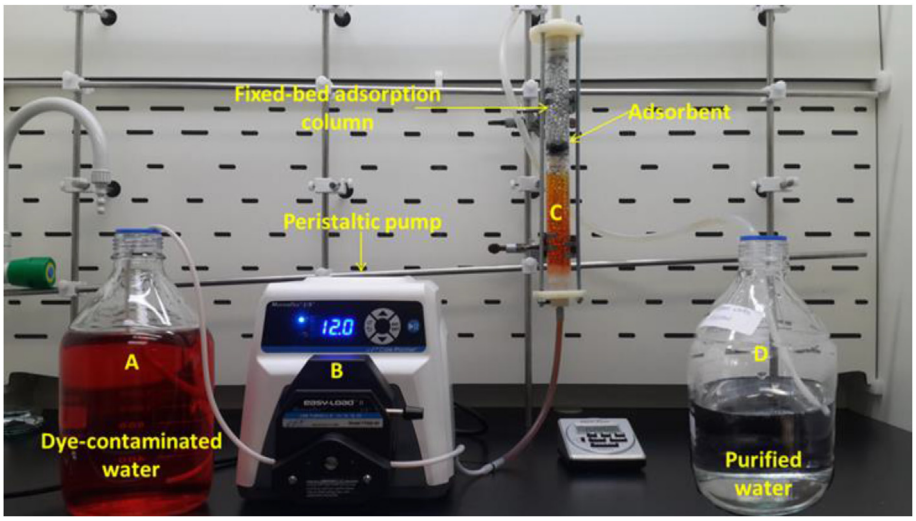

Figure 2. Photograph of column instrument setup.

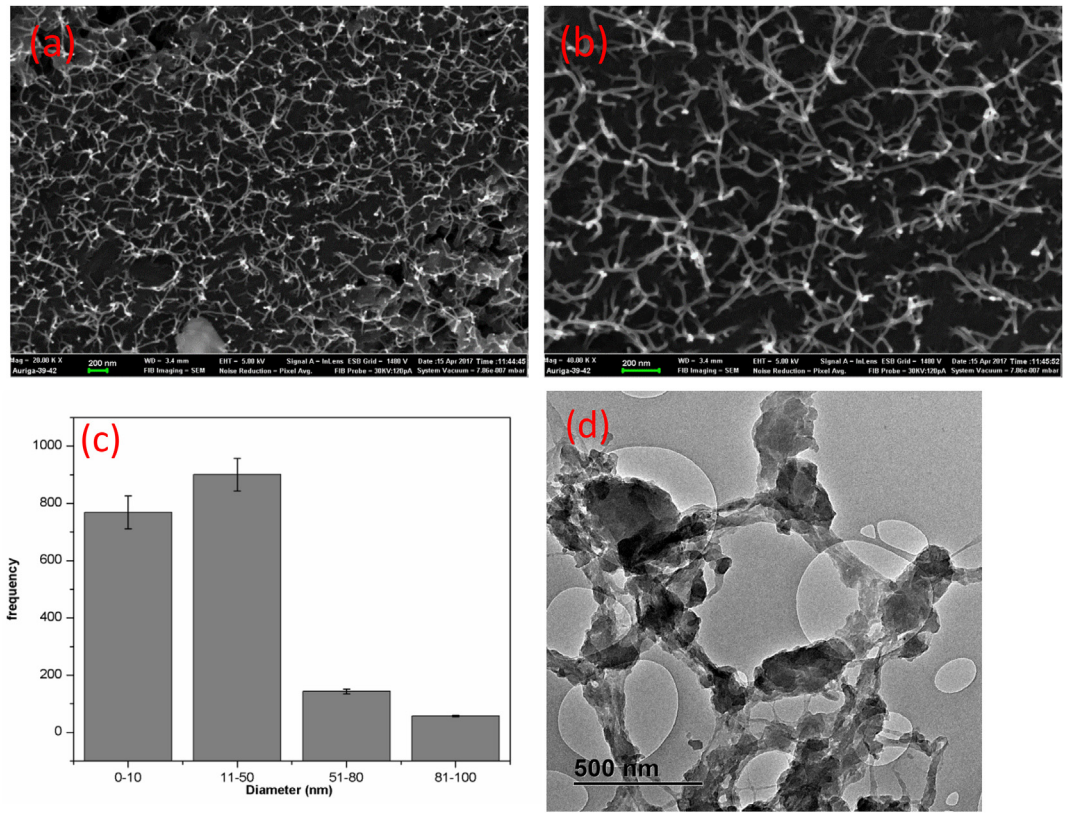

Figure 3. (a) and (b) FE-SEM images of PANI NFs at two different magnifications, (c) frequency bar chart for nanoparticles size of PANI NFs and (d) HR-TEM image of PANI NFs.

To quantify the MO molecules attached on the adsorbent at breakthrough point, q (mg) the following Eq. (3) is used [74]:

$$q = \frac{Q}{1000}\int_{t=0}^{t=t_b}(C_o - C_t)dt \tag{3}$$

Where Q in mL/min represents the volumetric flow rate, C_0 depicts the influent concentration in mg/L, t_b gives the time taken to reach breakthrough point (min) and C_t, represents the concentration of the effluent at any time, t mg/L [75]. Therefore, bed capacity at breakthrough point, q_b (mg/g) is calculated as shown in Eq. (4) [42, 76]:

$$q_b = \frac{q}{m} \tag{4}$$

where m represents the bed mass in grams.

2.4.2. Breakthrough curve modeling

The prediction of breakthrough curves is necessary to ascertain the success of a column process design. Also, a mandatory parameter for design is the maximum adsorbent capacity. The fixed-bed adsorption data may be fitted into several mathematical models. In a class of these models, the Thomas, Yoon-Nelson, and Bohart-Adams models [77, 78, 79] have been widely used by several researchers to characterize sorption processes in fixed-phase column adsorption experiments.

2.4.2.1. Thomas model. A model postulated by Thomas is commonly applied in describing the sorption performance theory in fixed-phase processes. It adopts a mass flow comportment in the bed and adherence to Langmuir adsorption-desorption isotherm model and reversible second-order kinetics [80]. Additionally, the model assumes limited restrictions from external and internal diffusions during the adsorption process [73]. This model is usually employed in calculating adsorption capacity, its linearized form is shown in Eq. (5) [78]:

$$\ln\left(\frac{C_o}{C_t} - 1\right) = k_{TH}q_o\frac{m}{Q} - k_{TH}C_o t \tag{5}$$

where, k_{TH} (mL/min mg) represents the rate constant and q_o in mg/g depicting adsorption capacity. The values for such parameters are obtainable from a linear plot of ln [(Co/Ct) −1] against time (t). Q denotes the inlet rate of solution flow in mL/min with m being the adsorbent mass in grams. The influent and effluent concentrations are represented by C_o and C_t, respectively (mg/L).

2.4.2.2. Yoon Nelson model. A model developed by Yoon and Nelson [81] assumes a proportional diminishing rate of adsorption prospect of an adsorbate molecule, in this case being MO, to the likelihood of adsorption and breakthrough of the adsorbate on the material bed [82]. Eq. (6) represents linearly the Yoon-Nelson model:

$$\ln\left(\frac{C_t}{C_o - C_t}\right) = k_{YN}t - k_{YN}\tau \tag{6}$$

From the equation, k_{YN} (min^{-1}) represents the Yoon-Nelson kinetic constant with τ (min) giving the period needed to achieve 50% breakthrough. C_o depicts the inlet concentration with C_t representing the effluent concentration. A linear plot of ln [C_t/(C_o−C_t)] versus sampling time (t) is employed in determining the k_{YN} and τ values using the intercept and slope respectively. Since the model assumes that 50% breakthrough is accomplished at time, τ, it, therefore, predicts that

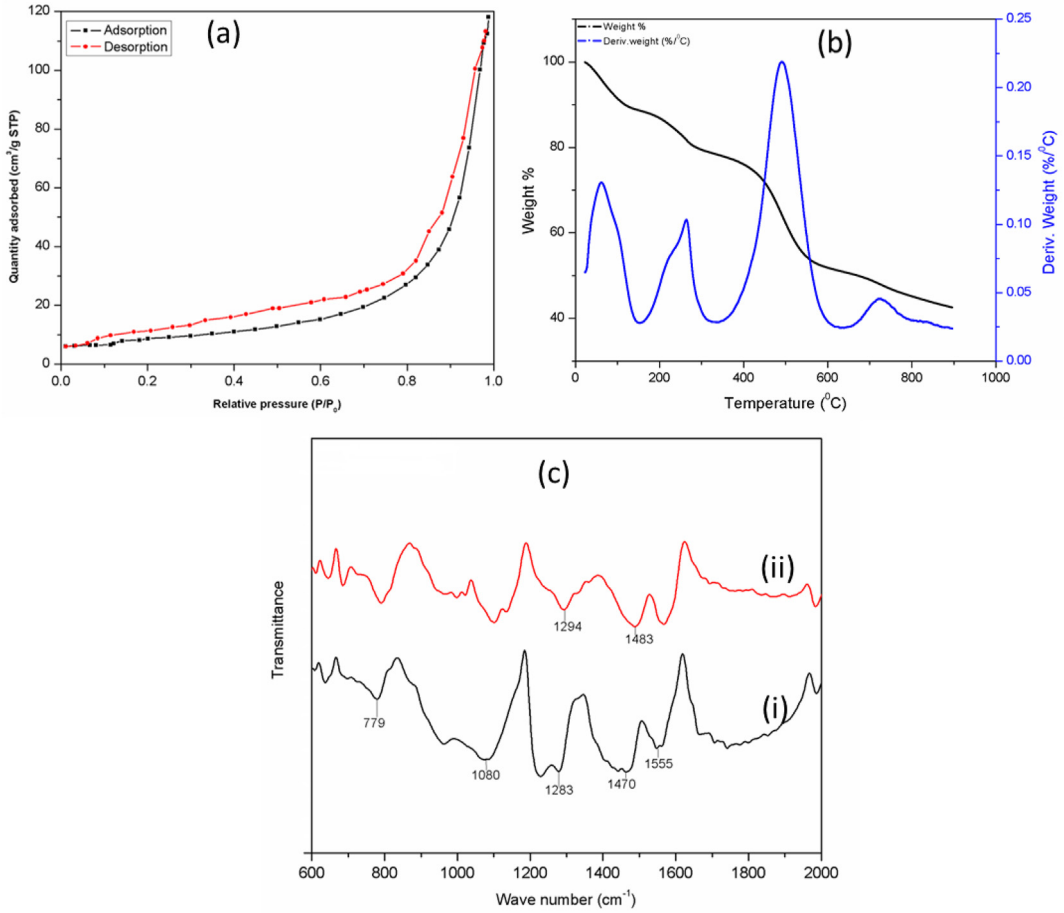

Figure 4. (a) N_2 adsorption–desorption curve of PANI NFs, (b) TGA curve for PANI NFs, and (c) ATR-FTIR spectrum of PANI NFs before (i) and after (ii) adsorption.

exhaustion of the adsorbent bed will be reached at time $= 2\tau$ which is attributed to the symmetrical form of the breakthrough curves [79].

2.4.2.3. Bohart-Adams model. Another model which is commonly used to evaluate the performance of an adsorption column process is the Bohart-Adams model. This model assumes a directly proportional relationship between the adsorption rate, the adsorbate molecule concentration, and the adsorbent's capacity for adsorption (Katsigiannis et al., 2015; Trgo et al., 2011). The model has been derived from reaction surface theory. It describes the early portion of the breakthrough curve and is mathematically depicted in the following Eq. (7):

$$ln\left(\frac{C_t}{C_o}\right) = k_{AB}C_o t - k_{AB}N_o\frac{Z}{U_o} \tag{7}$$

where k_{AB} (L/mg min) refers to the kinetic constant, N_o representing the concentration at saturation point in mg/L, and Z denoting the column height of the adsorbent in cm. U_o refers to the superficial velocity in cm/min, which is given by the flow rate (cm^3/min) proportion to the adsorbent bed's cross-sectional area (cm^2) [84].

2.5. Influence of process parameters

The influence of adsorbent bed length was investigated through altering the bed lengths at 3, 5.5, and 9 cm corresponding to 2, 4, and 6 g of the PANI NFs, respectively while maintaining a flow rate of 3 mL/min and influent concentration at 50 mg/L. In studies on the flow rate influence, the solution flow rates were varied at 3, 5, and 7 mL/min at 50 mg/L adsorbate influent concentration and 3 cm bed length. For experiments on the impact of influent concentration, the adsorbate concentration was varied at 25, 50, and 100 mg/L influent concentrations while maintaining a 3 cm adsorbent bed length and 3 mL/min flow rate.

2.6. Desorption and regeneration of PANI NFs

The desorption and regeneration of PANI NFs were accomplished using NaOH and HCl solutions, respectively. In a typical desorption process, 2 g mass (3 cm bed length) of the adsorbent was packed in a column and a 50 mg/L solution of MO was run to exhaustion at a flow rate of 3 mL/min. Subsequently, the exhausted adsorbent was treated with 1M NaOH solution until the effluent became almost colourless. The adsorbent was then treated with 1M hydrochloric acid to refurbish the PANI NFs with Cl^- and protonate the polyaniline to form a stable conformation. The regenerated adsorbent was subsequently employed in MO adsorption for several cycles, with the desorption procedure repeated after each adsorption cycle.

3. Results and discussion

3.1. Characterization of PANI NFs

3.1.1. Morphological characterization

Images from FE-SEM of the as-synthesized polyaniline nanofibers are shown in Figure 3(a) and (b). It is noted from Figure 3(c) that the PANI NFs have diameters that range from 10 to 80 nm. The PANI NFs also appear to have a surface that is smooth in texture. The HR-TEM demonstrated in Figure 3(d), also displays a morphology that is

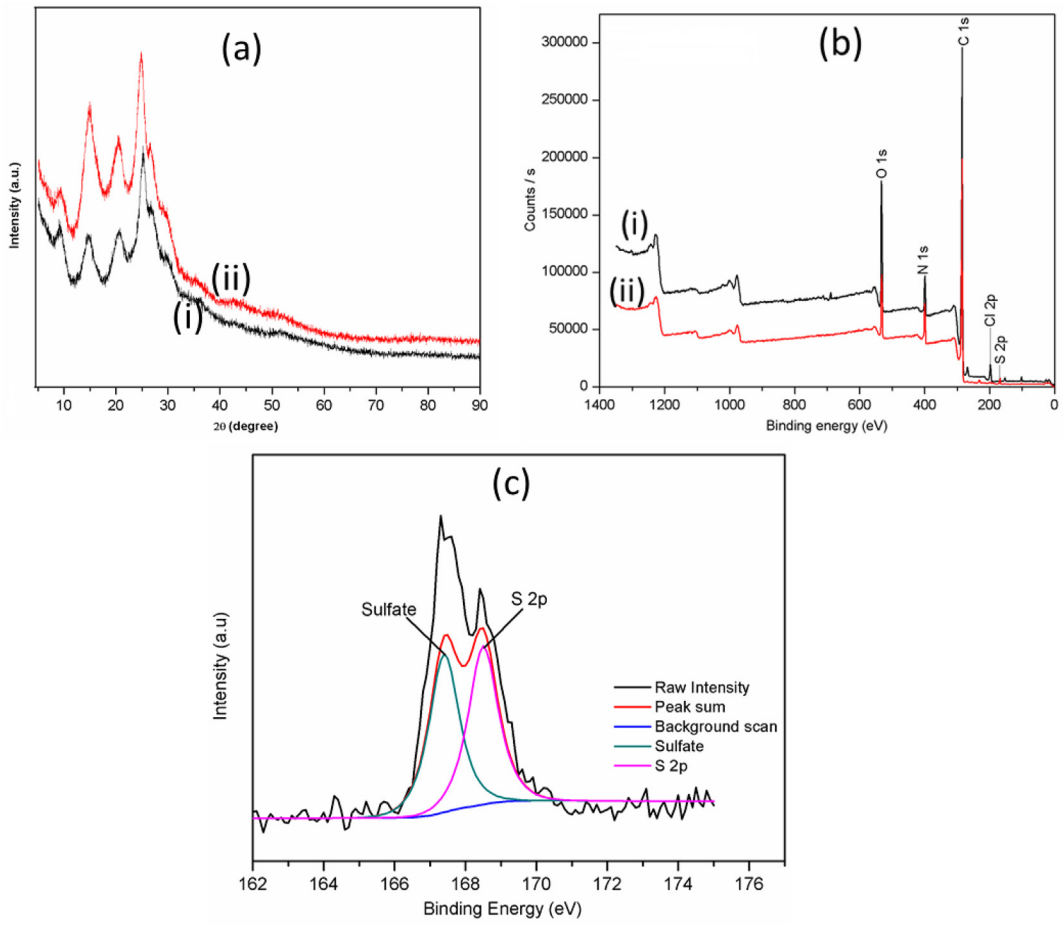

Figure 5. (a) XRD pattern of PANI NFs, (b) XPS spectrum for PANI NFs before (i) and after (ii) adsorption and (c) de-convoluted sulfur spectrum.

Table 1. Atomic percentage of elements before and after adsorption.

Elements	Atomic %	
	Before	After
C 1s	77.9	78.1
N 1s	6.0	9.9
Cl 2p	1.7	0.2
S 2p	0.0	1.0
O 1s	12.9	10.6

nanofibrous in nature. The micrographs further show agglomerates of the fibers into networks of nanofibers that are interconnected. Comparable structural features were similarly testified by Bhaumik *et al.* who prepared polyaniline nanofibers using the same technique as reported in this study [66]. Figure 4(a) illustrates the N_2 - adsorption–desorption isotherms of as-synthesized PANI NFs measured at -197.4 °C. A steep adsorption above the partial pressure of 0.8 is observed. This suggests that the PANI NFs are mesoporous in nature [28]. These curves were used to evaluate the BET surface area (S_{BET}) of the PANI NFs found to be 35.80 m^2/g. Also, the average pore diameter and volume of the adsorbent were respectively acquired to be 17.28 nm and 0.230 cm^3/g. The S_{BET} is comparable to that reported by Bhaumik *et al.* 38.99 m^2/g and higher than that of conventional PANI reported in other studies, i.e. 28.68 m^2/g [85].

3.1.2. Thermal stability profile of PANI NFs

Figure 4(b) shows the TGA curve of the PANI NFs. From this figure, a three-step decomposition process is eminent, and is consistent with that reported in the literature [63, 86, 87, 88, 89]. The weight loss observed at around 110 °C is caused by the vaporization of water and volatile oligomers. Unreacted monomers are also eliminated in this step. The next weight loss is observed between temperatures 280 °C and 450 °C. These weight losses may be ascribed to the degradation of the polymeric chain and the simultaneous exit of Cl^- counter ions, respectively.

3.1.3. Functional group analysis

The FTIR spectrum of pristine PANI NFs and after MO adsorption is presented in Figure 4(c). The spectrum portrays characteristic polyaniline signature peaks at 1555 cm^{-1}, 1470 cm^{-1}, 1283 cm^{-1}, 1080 cm^{-1} and 779 cm^{-1}. These peaks correspond to quinoid and benzenoid rings' stretching vibrations, vibrational stretching of C–N in quinoid-benzenoid-quinoid and benzenoid, benzenoid-NH^+ = quinoid stretching vibrations and vibrations of the deformation of aromatic C–H respectively. Comparable peaks have been reported in other studies i.e. 1568 cm^{-1}, 1490 cm^{-1}, 1276 cm^{-1}, and 1128 cm^{-1} for PANI (Bhaumik et al., 2016; Kerr et al., 2005). No significant difference in the spectra before and after MO adsorption was observed. However, a slight shift towards higher wavenumbers and reduced intensity in the peaks 1483 cm^{-1} and 1294 cm^{-1} is noted after adsorption. This can be accounted for by the substitution of SO_3^- from MO for doped Cl^- ions in the matrix of the polymer. It is conveyed in literature that resonant coupling with the

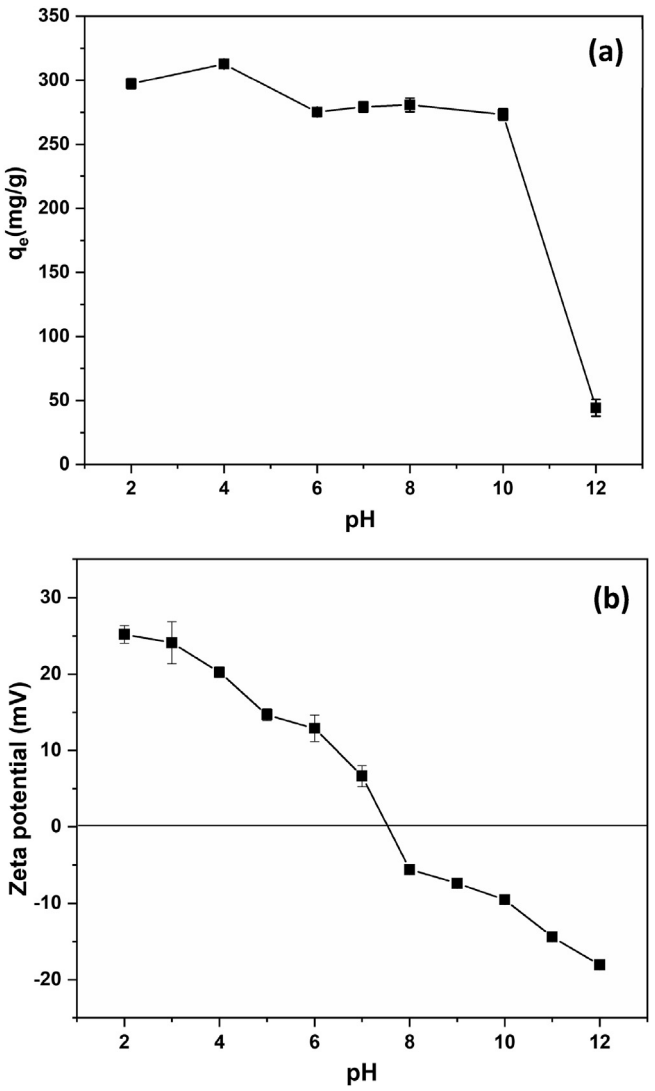

Figure 6. (a) Effect of pH on MO adsorption and (b) Zeta potential curve of PANI NFs at different pH values.

chain dopant may induce alterations in backbone vibrations and this could be responsible for the shifts and reduction in the intensity of FTIR peaks [66, 91].

Table 2. Comparison of maximum adsorption capacities (q_{max}) for MO on various adsorbents with present study.

Adsorbent	q_{max} (mg/g)	References
Amino-crosslinked hypromellose (AHM)	15.56	[34]
Blast furnace slag acid-alkali precipitate (BFSAP)	167	[94]
Protonated cross-linked chitosan	180.2	[95]
Coffee ground activated carbon	658	[96]
Waste ash	35.614	[36]
Chitosan-coated montmorillonite clay	7.34	[97]
Alkali-Activated Polypyrrole-Based Graphene Oxide	520.8	[98]
Manganese–containing mica (Mn–mica)	107.3	[35]
PANI NFs	312.8	Present study

3.1.4. Crystallographic and elemental analysis

XRD patterns of pristine PANI NFs and after adsorption are revealed in Figure 5(a). These patterns show emblematic PANI diffraction peaks centered at 2θ values of 9.1°, 14.7°, 20.6° and 25.1° (Wang et al., 2009; Tanwar and Ho, 2015). The pattern obtained after adsorption is not significantly different from that for pristine polyaniline indicating that the amorphous to slightly crystalline nature of the PANI NFs is not significantly altered by the adsorption of the dye. The incorporation of Cl, C, N, and O in the polymer, before MO adsorption, was confirmed by an XPS quantitative spectroscopic technique, as shown in Figure 5(b). The observed spectrum is similar to that reported by S. Tanwar and J. Annie Ho [93]. It can also be observed that after adsorption, a Sulfur (S) peak emerges (from the sulfate group in the MO structure) which is shown in the de-convoluted sulfur spectrum in Figure 5(c). Moreover, the intensity of C and N peaks increases with a slight decline in Cl peak intensity, which proves the attachment of the MO dye on the PANI NFs. Quantification of the elements is tabulated in Table 1.

3.1.5. Surface charge and pH stability of PANI NFs

The efficacy of an adsorbent in adsorption is considerably controlled by the pH of the adsorbate. The solution pH authorizes the overall surface charge and protonation of the adsorbent's functional groups. This parameter also has an effect on the extent of ionization and speciation of the substances which exist in the solution. Therefore, a preliminary batch adsorption investigation on pH impact was run to obtain the optimum pH for MO adsorption onto the PANI NFs. It is noted from Figure 6(a) that the adsorption of MO is less dependent on pH, but the adsorption efficiency slightly diminishes as the pH increases. The highest adsorption efficiency was observed at pH 4, with an equilibrium adsorption capacity, q_e of 312.8 mg/g in batch studies mode. This adsorption capacity for MO on PANI NFs is relatively higher compared to other adsorbents as presented in Table 2.

This influence of solution pH is explained in terms of surface charge effects. In this sense, the increase in MO decontamination at low pH may be elucidated with reference to the observed point of zero charge (PZC) or isoelectric point (pH_{PZC} = 7.5) of PANI NFs, Figure 6(b). At pH < pH_{PZC}, the release of doped Cl^- results in a positively charged PANI NFs surface. Additionally, excess H^+ protonates the nitrogen atoms in the polymer matrix thus contributing to the positively charged surface [99], affording probable success of the application of PANI NFs in textile effluent remediation. This suggests that the MO dye molecules were able to occupy vacant sites formerly occupied by Cl^- through ion exchange. At higher pH, however, the removal efficiency is reduced. This can be accredited to the expected nitrogen atoms' deprotonation in the PANI matrix, which results in less positively charged sites for the anionic dye attachment. Furthermore, at basic conditions, chemical affinity competition between the dye molecule's negatively charged (SO_3^-) groups and hydroxyl ions (OH^-) for active adsorption sites is more apparent (Bhaumik et al., 2013b; Bhaumik et al., 2013a).

3.2. Bed length effect

Adsorption depends on the adsorbent length (dosage) as this has an influence on the availability of active adsorption positions. To investigate the bed length influence on MO adsorption, the MO solution (50 mg/L concentration) was run through the adsorption column with a fixed rate of flow (3 mL/min) but fluctuating bed length at 3, 5.5, and 9 cm corresponding to 2, 4, and 6 g of the adsorbent, respectively (Figure 7). It is observed and confirmed in Figure 7 that there exists a dependence of breakthrough point with bed length. Increasing bed length results in enhanced availability of binding sites [100], hence the increase in the number of bed volumes processed, (*BV*) (1870–2105) and bed capacity, q_b (211.98–240.73 mg/g) depicted in Table 3. The longer residence time

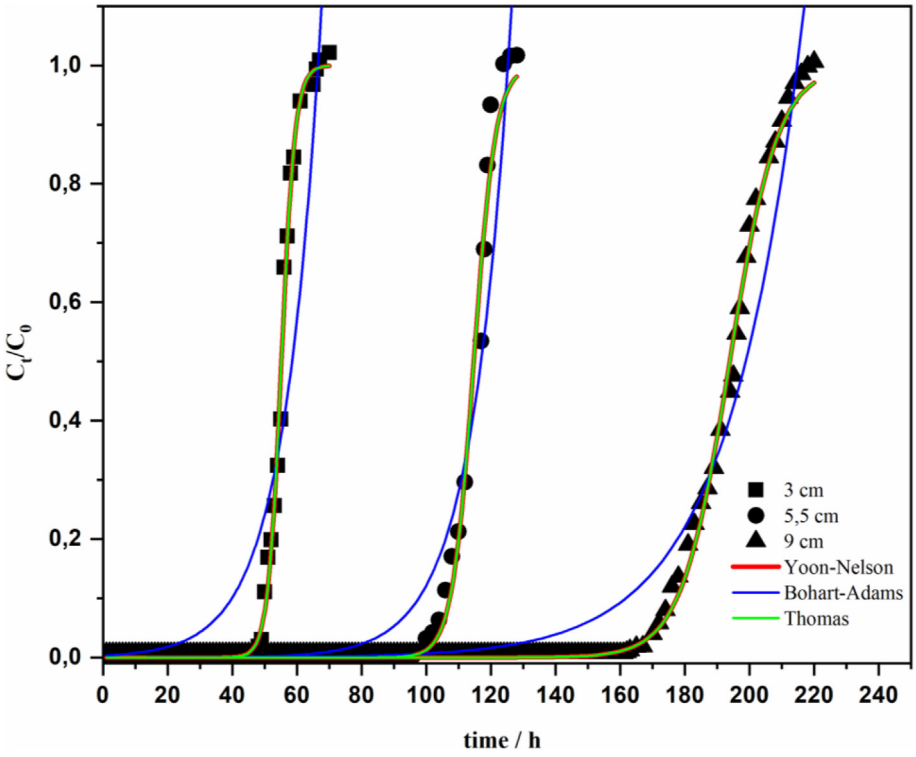

Figure 7. Effect of bed mass on MO removal.

of MO ions within the column bed in higher bed lengths may result in the observed bed capacity upsurge, hence larger volumes of MO solution could be treated. Presented in Table 3 are the values of the amount of solution treated at breakthrough point, (V_b) which were found to be 8.64 L, 17.64 L, and 29.16 L for bed lengths of 3, 5.5, and 9 cm, respectively. The observed increase may be allied to the rise in empty bed contact time, *EBCT* (from 1.54 to 4.62 min) which permits the MO ions sufficient diffusion time onto the PANI NFs [77]. The *EBCT* is the chief constraint that determines the adsorbate to adsorbent period of contact. Hence, *EBCT* will have a strong effect on the adsorption process [101]. *EBCT* is calculated as shown in Eq. (8):

$$\text{EBCT} = \frac{\text{Bed volume}}{\text{flow rate}} \tag{8}$$

Concurrently, the observed increase in breakthrough time (t_b) as bed length increases can be explained in terms of the fact that higher bed lengths encourage a decrease of slope in the breakthrough curve, and this results in broadened mass transfer zone [81]. On the other hand, the rate of exhaustion of the adsorbent, *AER* is reduced with a rise in bed length which indicates good column execution.

Table 3. Breakthrough point analysis.

Varied parameters	EBCT (min)	Service time,t_b (hrs)	V_b (L)	Capacity, q_b (mg/g)	Bed volume processed, (BV)	AER (g/L)
Adsorbent mass (g)						
2	1.54	48	8.64	211.98	1870	0.23
4	2.82	98	17.64	219.71	2085	0.23
6	4.62	162	29.16	240.73	2105	0.21
Influent conc. (mg/L)						
25	1.54	93	16.74	206.96	3623	0.12
50	1.54	48	8.64	211.98	1870	0.23
100	1.54	11	2.16	98.55	468	0.93
Flow rate (mL/min)						
3	1.54	48	8.64	211.98	1870	0.23
5	0.924	18	5.40	131.84	1169	0.37
7	0.66	11	4.62	114.25	1000	0.43

3.3. Flow rate effect

The contact time between the adsorbate and adsorbent in a packed column is influenced by the solution flow rate, thus making it a crucial parameter in the adsorption process. To inspect the flow rate impact; 3, 5, and 7 mL/min flow rates were used with the bed length and influent concentration fixed at 3 cm and 50 mg/L, respectively. Figure 8 illustrates the breakthrough curves for the different rates of solution flow. The curves exhibit a drop in breakthrough and saturation period with a rise in the rate of solution flow (Table 3). Breakthrough time values, t_b were established at 48, 18, and 11 h for 3, 5, and 7 mL/min flow rates, respectively. Short breakthrough times at higher flow rates were also reported by other researchers [102, 103, 104]. *BV* also decreased from 1870 to 1000 while *AER,* on the other hand, increased from 0.23 to 0.43 g/L with an increasing flow rate as shown in Table 3. Evidently, an increase in the rate of solution flow results in poor column performance.

Such results can be ascribed to reduced adsorbate residence period in the adsorbent bed with increasing flow rate; hence the time required for adequate diffusion of the MO ions onto the adsorbent bed becomes shorter. The increased flow rate also resulted in a decreased adsorption capacity, from 211.98 to 114.25 mg/g. Similarly, increasing the flow rate accelerates the MO transport through the column consequently limiting the exposure time of the dye molecules to the PANI NFs' active adsorption sites [41]. Similar results are reported in literature [80].

3.4. Influent concentration effect

To investigate the significance of inlet adsorbate concentration on MO adsorption, the bed length and rate of solution flow were maintained

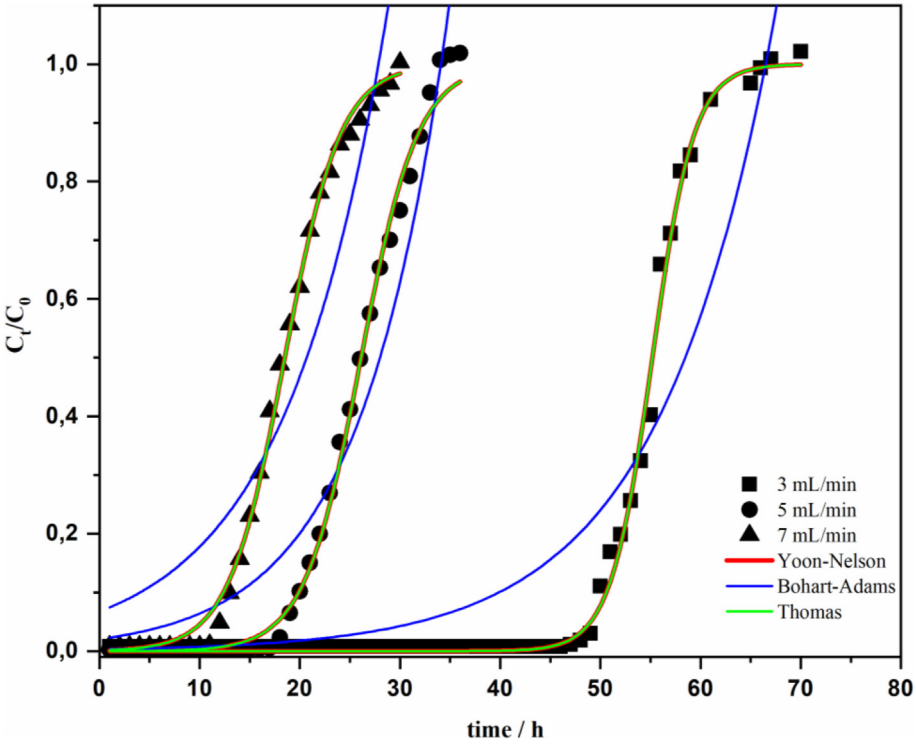

Figure 8. Effect of flow rate on MO removal.

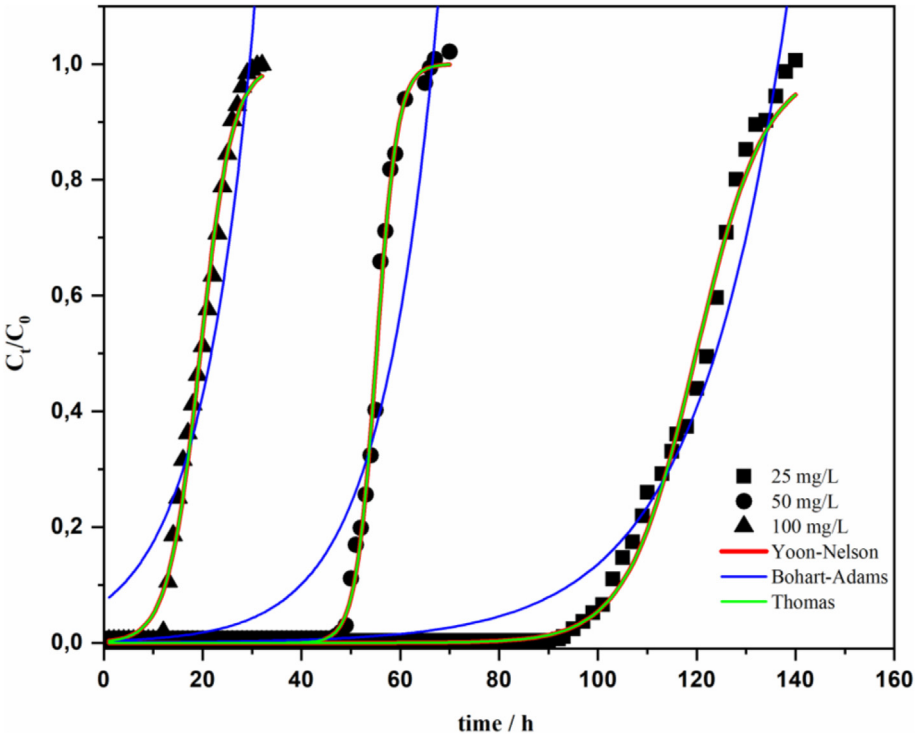

Figure 9. Effect of influent concentration on MO removal.

at 3 cm and 3 mL/min, respectively with the influent concentration varied at 25, 50, and 100 mg/L. The breakthrough curves shown in Figure 9 illustrates that increasing the influent concentration prompted a decrease in the breakthrough time resulting in lower volumes of water treated. V_b values were 16.74, 8.64, and 2.16 L for 25, 50, and 100 mg/L influent concentrations, respectively. A great dynamic force between the adsorbate and adsorbent prevails at pronounced inlet concentrations, resulting in improved mass transfer with a consequent increase in adsorbate exhaustion rate, due to high MO loading rate onto the PANI NFs' binding sites [81]. Similar trends were reported in the literature for chromium (VI) removal [70], fixed-bed adsorption of reactive azo dye [81], and several other studies [74, 82, 100, 103]. The breakthrough

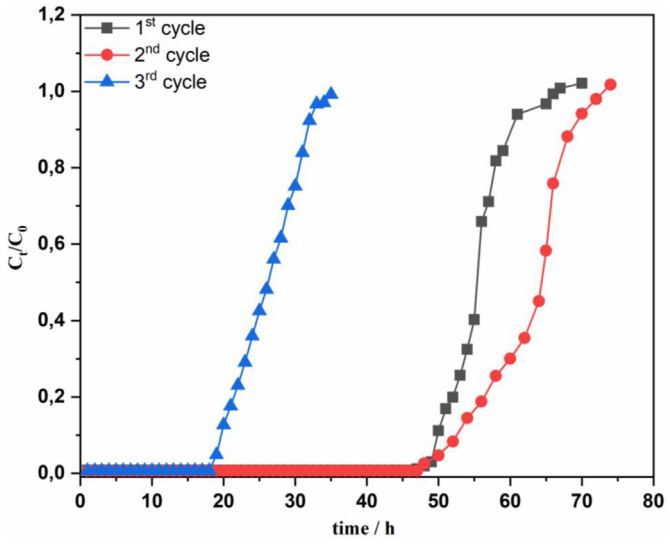

Figure 10. Adsorption curve for different cycles after desorption.

point was reached after 93, 48, and 11 h for the influent concentration of 25, 50, and 100 mg/L, respectively. Table 3 presents the breakthrough parameters.

3.5. Desorption of MO and adsorbent regeneration

Facile regeneration of a sorbent is very important for economic stability. In accordance with the effect of surface charge on the adsorption efficiency, it was considered that an alkali solution could be employed to discern the desorption of the adsorbed MO dye. It is expected that the anionic nature of the polymer matrix increases when it is subjected to basic conditions, and thus enabling electrostatic repulsion of the dye anions. This may serve as the basis for the dye elution off the polymer [105]. Figure 10 shows the adsorption breakthrough curves for 3 cycles. It is observed that the first and second cycles of adsorption took 48 h to attain the breakthrough point with the third cycle reaching breakthrough at 18 h. Accordingly, exposing the polyaniline to HCl after treatment with NaOH successfully refurbished the PANI NFs with Cl^- and replenished the stable protonated conformation (emeraldine) of the polyaniline nanofibers, hence the observed recyclability potential of the adsorbent [106, 107]. The recyclability of the PANI NFs qualifies it as a re-useable sorbent possessing good adsorption capacity and stability for MO decontamination from water.

3.6. Breakthrough curve modeling

The column adsorption data were fitted in three breakthrough adsorption models, viz Thomas, Yoon-Nelson, and Bohart-Adams models, and the results are presented in Table 4.

3.6.1. Thomas model

The Thomas model was fitted in equilibrium data, and it yielded high R^2 values (0.914–0.978) suggesting that the adsorption may follow Thomas model equilibrium dynamics. Respectively, Table 4 demonstrates a rise in q_o as the adsorbent length increased, possibly due to the affordable availability of more sorption sites. However, q_o values lessened with rising flow rate and inlet concentration, which may be as a result of decreased adsorbate residence time and higher driving force leading to early adsorbate saturation, respectively [42]. Conversely, k_{TH} values generally diminished with an upsurge of flow rate, bed length, and influent concentration.

3.6.2. Yoon Nelson model

Inspection data were also fitted into the Yoon-Nelson model and high R^2 values were obtained (0.939–0.986), suggesting the possibility of the removal of MO using PANI NFs following this ideal. Comparing investigational saturation times with calculated values of 2τ, the two values are very close to each other thus confirming the applicability of Yoon-Nelson model for adsorption of MO by PANI NFs. Furthermore, as revealed in Table 4, the calculated R^2 values (0.939–0.986) rule over others from investigated models. τ values improved with bed length owing to more adsorption sites accessibility, yet conversely, the τ values diminished with a rise in flow rate and influent concentration. This decrease in τ values is possibly explained by the expected rise in saturation rate of the PANI NFs adsorbent as the flow rate and influent concentration increase. There was an observed rise in k_{YN} values as influent concentration increased and this ascribes to the improved bulk transfer rate that prevails at such experimental conditions [79]. Increasing bed length, however, resulted in low k_{YN} values.

3.6.3. Bohart-Adams model

For the Bohart-Adams model fitting, Table 4 shows relatively low regression coefficient (R^2) values (0.640–0.9403), and this signifies that this model does not provide a good representation of the MO adsorption using PANI NFs equilibrium dynamics. The values of k_{AB} and N_o were fluctuating as the parameters were varied.

4. Conclusion

In this study, polyaniline nanofibers fabricated via quick mixing chemical oxidative polymerization were investigated for their potential

Table 4. Fixed-bed column modeling parameters.

	Thomas model			Bohart-Adams			Yoon-Nelson		
Parameters	K_{TH} x10^{-3}	q_0	R^2	K_{BA} x10^{-3}	N_0	R^2	K_{YN}	τ	R^2
Bed mass									
2	9.389	4165.14	0.914	4.91	2972.78	0.782	0.469	55.54	0.980
4	7.173	4261.98	0.948	6.248	2877.31	0.931	0.349	113.70	0.947
6	3.053	4798.93	0.952	1.746	3348.01	0.891	0.155	190.02	0.963
Flow rate									
3	11.148	3889.53	0.975	8.562	2762.08	0.940	0.5467	52.93	0.986
5	8.834	3438.14	0.945	5.708	2447.63	0.811	0.4289	26.45	0.948
7	7.826	3391.91	0.953	4.548	2768.19	0.757	0.3913	13.38	0.953
Influent concentration									
25	6.628	4452.25	0.968	3.808	3137.15	0.881	0.1657	118.73	0.968
50	9.416	4165.62	0.978	4.91	2972.78	0.782	0.4708	55.54	0.978
100	4.406	2943.58	0.939	1.682	2652.71	0.640	0.4406	19.62	0.939

in decontamination of methyl orange dye from water via a fixed-bed column adsorption set-up. The as-synthesized PANI NFs exhibited a smooth homogeneous interconnection of nanometer-sized fibers, with a relatively high average surface area (35.80 m^2/g). The MO decontamination results revealed that optimum MO removal is favoured by low influent concentration and rate of solution flow with high bed length. Adsorption of the MO was afforded by electrostatic interactions of the protonated PANI NFs surfaces and anionic methyl orange SO_3^- groups. The bed volumes, *BV* processed, increased with bed length. Contrarily, *BV* drops with a rise in both flow rate and influent concentration. The rate of adsorbent exhaustion, *AER* rises with the rate of solution flow and inlet concentration. The Thomas and Yoon-Nelson mathematical models yielded a good correlation with the column data whereas the Bohart-Adams model gave a poor fit. Ultimately, the results show that 6 g (bed length = 9 cm) of PANI NFs can readily treat 29.16 L of 25 mg/L MO solution at a flow rate of 3 mL/min attaining the breakthrough point at 162 h. Additionally, the adsorbent can be used in more than one cycle before being recycled. Therefore, PANI NFs are effective as potential adsorbents for MO removal in fixed-bed operation techniques.

Declarations

Author contribution statement

Mbongiseni Lungelo Dlamini: Performed the experiments; Analyzed and interpreted the data.

Madhumita Bhaumik: Conceived and designed the experiments; Analyzed and interpreted the data.

Kriveshini Pillay: Conceived and designed the experiments; Analyzed and interpreted the data; Contributed reagents, materials, analysis tools or data.

Arjun Maity: Conceived and designed the experiments; Analyzed and interpreted the data; Contributed reagents, materials, analysis tools or data.

Funding statement

This work was supported by the National Research Foundation.

Data availability statement

No data was used for the research described in the article.

Declaration of interests statement

The authors declare no conflict of interest.

Additional information

No additional information is available for this paper.

Acknowledgements

The authors appreciatively acknowledge the DST/CSIR National Centre for Nanostructured Materials characterization unit for assisting with materials characterization.

References

[1] S. Mani, R.N. Bharagava, 3 Textile Industry Wastewater Environmental and Health Hazards and Treatment Approaches, 2018.
[2] M. Behera, J. Nayak, S. Banerjee, S. Chakrabortty, S.K. Tripathy, A review on the treatment of textile industry waste effluents towards the development of efficient mitigation strategy: an integrated system design approach, J. Environ. Chem. Eng. 9 (2021) 105277.
[3] L.D. Ardila-Leal, R.A. Poutou-Piñales, A.M. Pedroza-Rodríguez, B.E. Quevedo-Hidalgo, A brief history of colour, the environmental impact of synthetic dyes and removal by using laccases, Molecules 26 (2021) 3813.
[4] T. Toprak, P. Anis, Textile industry's environmental effects and approaching cleaner production and sustainability: an overview, J. Text. Eng. Fash. Technol. 2 (2017) 429–442.
[5] M. Berradi, R. Hsissou, M. Khudhair, M. Assouag, O. Cherkaoui, A. El Bachiri, A. El Harfi, Textile finishing dyes and their impact on aquatic environs, Heliyon 5 (2019).
[6] Y. Yang, C. Guan, Adsorption properties of activated carbon fiber for highly effective removal of methyl orange dye, IOP Conf. Ser. Earth Environ. Sci. 208 (2018).
[7] S. Samsami, M. Mohamadi, M.H. Sarrafzadeh, E.R. Rene, M. Firoozbahr, Recent advances in the treatment of dye-containing wastewater from textile industries: overview and perspectives, Process Saf. Environ. Protect. 143 (2020) 138–163.
[8] S.A. Butani, S.J. Mane, Coagulation/flocculation process for cationic, anionic dye removal using water treatment residuals – a review, Int. J. Serv. Technol. Manag. 6 (2017) 1–5.
[9] G. Han, C.Z. Liang, T.S. Chung, M. Weber, C. Staudt, C. Maletzko, Combination of forward osmosis (FO) process with coagulation/flocculation (CF) for potential treatment of textile wastewater, Water Res. 91 (2016) 361–370.
[10] J.A. Garrido-Cardenas, B. Esteban-García, A. Agüera, J.A. Sánchez-Pérez, F. Manzano-Agugliaro, Wastewater treatment by advanced oxidation process and their worldwide research trends, Int. J. Environ. Res. Publ. Health 17 (2020).
[11] R. Javaid, U.Y. Qazi, Catalytic oxidation process for the degradation of synthetic dyes: an overview, Int. J. Environ. Res. Publ. Health 16 (2019) 1–27.
[12] N. Klanovicz, A.F. Camargo, F.S. Stefanski, J. Zanivan, T. Scapini, R. Pollon, A. Warken, L. Paliga, K.P. Preczeski, A.A.G.A. Ribeiro, J. Garda-Buffon, G. Fongaro, H. Treichel, Advanced oxidation processes applied for color removal of textile effluent using a home-made peroxidase from rice bran, Bioproc. Biosyst. Eng. 43 (2020) 261–272.
[13] S. Ledakowicz, K. Pázdzior, Recent achievements in dyes removal focused on advanced oxidation processes integrated with biological methods, Molecules 26 (2021).
[14] M.M. Hassan, C.M. Carr, A critical review on recent advancements of the removal of reactive dyes from dyehouse effluent by ion-exchange adsorbents, Chemosphere 209 (2018) 201–219.
[15] E. Polska-Adach, M. Wawrzkiewicz, Z. Hubicki, Removal of acid, direct and reactive dyes on the polyacrylic anion exchanger, Physicochem. Probl. Miner. Process. 55 (2019) 1496–1508.
[16] M.A. Khan, M.I. Khan, S. Zafar, Removal of different anionic dyes from aqueous solution by anion exchange membrane, Membr. Water Treat. 8 (2017) 259–277.
[17] M. Agtaş, T. Ormancı-Acar, B. Keskin, T. Türken, I. Koyuncu, Nanofiltration membranes for salt and dye filtration: effect of membrane properties on performances, Water Sci. Technol. 83 (2021) 2146–2159.
[18] A.M. Hidalgo, M.D. Murcia, Membranes for water and wastewater treatment, Membranes 11 (2021) 9–14.
[19] M. Sala, M.C. Gutiérrez-Bouzán, Electrochemical techniques in textile processes and wastewater treatment, Int. J. Photoenergy 2012 (2012).
[20] T. Shindhal, P. Rakholiya, S. Varjani, A. Pandey, H.H. Ngo, W. Guo, H.Y. Ng, M.J. Taherzadeh, A critical review on advances in the practices and perspectives for the treatment of dye industry wastewater, Bioengineered 12 (2021) 70–87.
[21] A. Bellifa, M. Makhlouf, Z.H. Boumila, Comparative study of the adsorption of methyl orange by bentonite and activated carbon, Acta Phys. Pol., A 132 (2017) 466–468.
[22] Y. Wang, Q. Geng, J. Yang, Y. Liu, C. Liu, Hybrid system of flocculation-photocatalysis for the decolorization of crystal violet, reactive red X-3B, and acid orange II dye, ACS Omega 5 (2020) 31137–31145.
[23] S. Moosavi, R.Y.M. Li, C.W. Lai, Y. Yusof, S. Gan, O. Akbarzadeh, Z.Z. Chowhury, X.G. Yue, M.R. Johan, Methylene blue dye photocatalytic degradation over synthesised fe3 o4/ac/tio2 nano-catalyst: degradation and reusability studies, Nanomaterials 10 (2020) 1–15.
[24] G. Dogdu Okcu, T. Tunacan, E. Dikmen, Removal of indigo dye by photocatalysis process using Taguchi experimental design, Environ. Res. Technol. (2019).
[25] G. Chandrabose, A. Dey, S.S. Gaur, S. Pitchaimuthu, H. Jagadeesan, N.S.J. Braithwaite, V. Selvaraj, V. Kumar, S. Krishnamurthy, Removal and degradation of mixed dye pollutants by integrated adsorption-photocatalysis technique using 2-D MoS2/TiO2 nanocomposite, Chemosphere 279 (2021) 130467.
[26] E.O. Ezugbe, S. Rathilal, Membrane technologies in wastewater treatment: a review, Membranes 10 (2020).
[27] N.Y. Donkadokula, A.K. Kola, I. Naz, D. Saroj, A review on advanced physico-chemical and biological textile dye wastewater treatment techniques, Rev. Environ. Sci. Biotechnol. 19 (2020) 543–560.
[28] Q. Xin, J. Fu, Z. Chen, S. Liu, Y. Yan, J. Zhang, Q. Xu, Polypyrrole nanofibers as a high-efficient adsorbent for the removal of methyl orange from aqueous solution, J. Environ. Chem. Eng. 3 (2015) 1637–1647.
[29] M. Kaykhaii, M. Sasani, S. Marghzari, Removal of dyes from the environment by adsorption process, Chem. Mater. Eng. 6 (2018) 31–35.
[30] E. Okoniewska, Removal of selected dyes on activated carbons, Sustain. Times 13 (2021).
[31] R. Lafi, A. Hafiane, Removal of methyl orange (MO) from aqueous solution using cationic surfactants modified coffee waste (MCWs), J. Taiwan Inst. Chem. Eng. 58 (2016) 424–433.
[32] A. Agarwal, Vaishali, Removal of methyl orange dye from textile effluent using adsorption on chitosan hydrogel beads, ESSENCE - Int. J. Environ. Rehabil. Conserv. VII (2016) 73–80.
[33] R. Istratie, M. Stoia, C. Păcurariu, C. Locovei, Single and simultaneous adsorption of methyl orange and phenol onto magnetic iron oxide/carbon nanocomposites, Arab. J. Chem. 12 (2019) 3704–3722.

[34] W. Qu, D. He, H. Huang, Y. Guo, Y. Tang, R.J. Song, Characterization of amino-crosslinked hypromellose and its adsorption characteristics for methyl orange from water, J. Mater. Sci. 55 (2020) 7268–7282.
[35] M.A. Barakat, A.Q. Selim, M. Mobarak, R. Kumar, I. Anastopoulos, D. Giannakoudakis, A. Bonilla-Petriciolet, E.A. Mohamed, M.K. Seliem, S. Komarneni, Experimental and theoretical studies of methyl orange uptake by mn–rich synthetic mica: insights into manganese role in adsorption and selectivity, Nanomaterials 10 (2020) 1–17.
[36] S. Savci, M.M. Uysal, Adsorption of methylene blue and methyl orange by using waste ash, Süleyman Demirel Üniv. Fen Bilim. Enstitüsü Derg. 21 (2017) 831.
[37] S.S. Shah, T. Sharma, B.A. Dar, R.K. Bamezai, Adsorptive removal of methyl orange dye from aqueous solution using populous leaves: insights from kinetics, thermodynamics and computational studies, Environ. Chem. Ecotoxicol. 3 (2021) 172–181.
[38] T.C. Egbosiuba, A.S. Abdulkareem, A.S. Kovo, E.A. Afolabi, J.O. Tijani, M.T. Bankole, S. Bo, W.D. Roos, Adsorption of Cr(VI), Ni(II), Fe(II) and Cd(II) ions by KIAgNPs decorated MWCNTs in a batch and fixed bed process, Sci. Rep. 11 (2021) 1–20.
[39] N. Ye, N. Cimetiere, V. Heim, N. Fauchon, C. Feliers, D. Wolbert, Upscaling fixed bed adsorption behaviors towards emerging micropollutants in treated natural waters with aging activated carbon: model development and validation, Water Res. 148 (2019) 30–40.
[40] M. Badrelzaman, M.I. Khamis, T.H. Ibrahim, F.H. Jumean, Scale-up of self-regenerating semi-batch adsorption cycles through concurrent adsorption and reduction of Cr(VI) on sheep wool, Processes 8 (2020) 1–10.
[41] P.R. Rad, A. Fazlali, Optimization of permeable reactive barrier dimensions and location in groundwater remediation contaminated by landfill pollution, J. Water Process Eng. 35 (2020).
[42] Y. Zhang, F. Jin, Z. Shen, F. Wang, R. Lynch, A. Al-Tabbaa, Adsorption of methyl tert-butyl ether (MTBE) onto ZSM-5 zeolite: fixed-bed column tests, breakthrough curve modelling and regeneration, Chemosphere 220 (2019) 422–431.
[43] V. Manirethan, R.M. Balakrishnan, Batch and continuous studies on the removal of heavy metals using biosynthesised melanin impregnated activated carbon, Environ. Technol. Innov. 20 (2020) 24723–24737.
[44] N. Sazali, Z. Harun, N. Sazali, A review on batch and column adsorption of various adsorbent towards the removal of heavy metal, J. Adv. Res. Fluid Mech. Therm. Sci. 67 (2020) 66–88.
[45] Z. Karimi, R. Khalili, M. Ali Zazouli, Surface modified polythiophene/Al2O3 and polyaniline/Al2O3 nanocomposites using poly(vinyl alcohol) for the removal of heavy metal ions from water: kinetics, thermodynamic and isotherm studies, Water Sci. Technol. 84 (2021) 182–199.
[46] M.M. Ayad, W.A. Amer, S. Zaghlol, I.M. Minisy, P. Bober, J. Stejskal, Polypyrrole-coated cotton textile as adsorbent of methylene blue dye, Chem. Pap. 72 (2018) 1605–1618.
[47] A.H. Birniwa, A.S. Abubakar, A.K.O. Huq, H.N.M.E. Mahmud, Polypyrrole-polyethyleneimine (PPy-PEI) nanocomposite: an effective adsorbent for nickel ion adsorption from aqueous solution, J. Macromol. Sci. Part A Pure Appl. Chem. 58 (2021) 206–217.
[48] M. Duhan, R. Kaur, Nano-structured polyaniline as a potential adsorbent for methylene blue dye removal from effluent, J. Compos. Sci. 5 (2021).
[49] J. Chen, J. Zhu, N. Wang, J. Feng, W. Yan, Hydrophilic polythiophene/SiO 2 composite for adsorption engineering: green synthesis in aqueous medium and its synergistic and specific adsorption for heavy metals from wastewater, Chem. Eng. J. 360 (2019) 1486–1497.
[50] J. Chen, N. Wang, H. Ma, J. Zhu, J. Feng, W. Yan, Facile modification of a polythiophene/TiO2 composite using surfactants in an aqueous medium for an enhanced Pb(II) adsorption and mechanism investigation, J. Chem. Eng. Data 62 (2017) 2208–2221.
[51] P. Khalaj, H. Naghibi, M. Ghorbani, Polypyrrole coated tin oxide nanocomposite: an efficient dye adsorbent and microbial disinfectant, J. Dispersion Sci. Technol. (2020) 1–13, 0.
[52] A. Nasar, F. Mashkoor, Application of polyaniline-based adsorbents for dye removal from water and wastewater—a review, Environ. Sci. Pollut. Res. 26 (2019) 5333–5356.
[53] D. Thanasamy, D. Jesuraj, S.K. Konda kannan, V. Avadhanam, A novel route to synthesis polythiophene with great yield and high electrical conductivity without post doping process, Polymer 175 (2019) 32–40.
[54] T.H. Le, Y. Kim, H. Yoon, Electrical and electrochemical properties of conducting polymers, Polymers 9 (2017).
[55] F. Nastase, Introductory chapter: polyaniline - from synthesis to practical applications, polyaniline - from synth. To Pract. Appl. [Working Title], 2019.
[56] S.K. Moosvi, F.A. Rafiqi, Brief Discussion on the Properties and Applications of Polypyrrole and Polythiophene Conducting Polymer, 2019.
[57] A. Husain, S. Ahmad, F. Mohammad, Preparation and Applications of Polythiophene Nanocomposites 1, 2020, pp. 36–53.
[58] M. Beygisangchin, S.A. Rashid, S. Shafie, A.R. Sadrolhosseini, Polyaniline Thin Films — A Review, 2021.
[59] N. Mahato, H. Jang, A. Dhyani, S. Cho, Recent Progress in Conducting Polymers for Hydrogen Storage and Fuel Cell Applications, 2020.
[60] A.K. Mishra, Conducting polymers: concepts and applications, J. At. Mol. Condens. Nano Phys. 5 (2018) 159–193.
[61] K. Namsheer, C.S. Rout, Conducting polymers: a comprehensive review on recent advances in synthesis, properties and applications, RSC Adv. 11 (2021) 5659–5697.
[62] N. Amariei, L.R. Manea, A.P. Bertea, R. Cramariuc, A. Bertea, O. Cramariuc, Electrospinning polyaniline for sensors, IOP Conf. Ser. Mater. Sci. Eng. 209 (2017).
[63] A.R. Phani, R.D.B.M. T, S. Srinivasan, L. Stefanakos, Polyaniline nanofibers obtained by electrospin process for hydrogen, Storage Appl. 4 (2014) 375–386.
[64] Y. Wang, Preparation and application of polyaniline nanofibers: an overview, Polym. Int. 67 (2018) 650–669.
[65] A. Abdolahi, E. Hamzah, Z. Ibrahim, S. Hashim, Synthesis of uniform polyaniline nanofibers through interfacial polymerization, Materials 5 (2012) 1487–1494.
[66] M. Bhaumik, R.I. McCrindle, A. Maity, S. Agarwal, V.K. Gupta, Polyaniline nanofibers as highly effective re-useable adsorbent for removal of reactive black 5 from aqueous solutions, J. Colloid Interface Sci. 466 (2016) 442–451.
[67] R.E. Morsi, E.A. Khamis, A.M. Al-Sabagh, Polyaniline nanotubes: facile synthesis, electrochemical, quantum chemical characteristics and corrosion inhibition efficiency, J. Taiwan Inst. Chem. Eng. 60 (2016) 573–581.
[68] J. Manuel, T. Salguero, R.P. Ramasamy, Synthesis and characterization of polyaniline nanofibers as cathode active material for sodium-ion battery, J. Appl. Electrochem. 49 (2019) 529–537.
[70] M. Bhaumik, K. Setshedi, A. Maity, M.S. Onyango, Removal from water using fixed bed column of polypyrrole/Fe 3O4 nanocomposite, Separ. Purif. Technol. 110 (2013) 11–19.
[71] M.R. Gadekar, M.M. Ahammed, Use of water treatment residuals for colour removal from real textile dye wastewater, Appl. Water Sci. 10 (2020) 1–8.
[72] M.S. Onyango, T.Y. Leswifi, A. Ochieng, D. Kuchar, F.O. Otieno, H. Matsuda, Breakthrough analysis for water defluoridation using surface-tailored zeolite in a fixed bed column, Ind. Eng. Chem. Res. 48 (2009) 931–937.
[73] K.Z. Setshedi, M. Bhaumik, M.S. Onyango, A. Maity, Breakthrough studies for Cr(VI) sorption from aqueous solution using exfoliated polypyrrole-organically modified montmorillonite clay nanocomposite, J. Ind. Eng. Chem. 20 (2013) 2208–2216.
[74] U. Maheshwari, S. Gupta, Removal of Cr(VI) from wastewater using activated neem bark in a fixed-bed column: interference of other ions and kinetic modelling studies, Desalin. Water Treat. 57 (2016) 8514–8525.
[75] M. Dutta, J.K. Basu, H. Faraz, N. Gautam, A. Kumar, Fixed-bed column study of textile dye direct blue 86 by using A composite, Adsorbent 4 (2012) 882–891.
[76] M. Yadav, P. Tripathi, A. Choudhary, U. Brighu, S. Mathur, Adsorption of fluoride from aqueous solution by Bio-F sorbent: a fixed-bed column study, Desalin. Water Treat. 3994 (2015). Ahead of Print.
[77] S. Song, Y. Hau, N. Saman, K. Johari, S. Cheu, H. Kong, H. Mat, Process analysis of mercury adsorption onto chemically modi fi ed rice straw in a fi xed-bed adsorber, J. Environ. Chem. Eng. Cont. Biochem. Pharmacol. 4 (2016) 1685–1697.
[78] S. Noreen, H.N. Bhatti, Z. Farrukh, S. Ilays, M.A. Jamal, Continuous fixed bed removal of Novacron Orange P-2R using sugarcane bagasse: prediction of breakthrough curves, Desalin. Water Treat. 57 (2016) 12814–12821.
[79] A. Katsigiannis, C. Noutsopoulos, J. Mantziaras, M. Gioldasi, Removal of emerging pollutants through granular activated carbon, Chem. Eng. J. 280 (2015) 49–57.
[80] J.H.C.J. Ma, F. Yu, L. Zhou, L. Jin, M.X. Yang, J.S. Luan, Y.H. Tang, H.B. Fan, Z.W. Yuan, Enhanced adsorption removal of methyl orange and methylene blue from aqueous solution by alkali-activated multiwalled carbon nanotubes, Appl. Mater. Interf. (2012) 5749–5760.
[81] A.A. Ahmad, B.H. Hameed, Fixed-bed adsorption of reactive azo dye onto granular activated carbon prepared from waste, J. Hazard Mater. 175 (2010) 298–303.
[82] E. Oguz, M. Ersoy, Removal of Cu2+ from aqueous solution by adsorption in a fixed bed column and Neural Network Modelling, Chem. Eng. J. 164 (2010) 56–62.
[84] Usace, Adsorption Design Guide, 1110-1111–2, 2001, pp. 1–1111.
[85] S. Budi, E. Fitri, M. Paristiowati, U. Cahyana, E. Pusparini, H. Nasbey, A. Imaddudin, Surface area and conductivity of polyaniline synthesized under UV irradiation, J. Phys. Conf. Ser. Mater. Sci. Eng. 172 (2017) 755.
[86] O. Nanocomposites, A.M. Díez-pascual, J.A. Luceño-sánchez, Development and Characterization of Polyaniline/Hexamethylene Diisocyanate-Modified Graphene, 2021.
[87] E. Baştürk, E. Çakmakçi, S. Madakbaş, M.V. Kahraman, Surface and proton conductivity properties of electrospun poly(vinyl butyral)/polyaniline nanofibers, Adv. Polym. Technol. 37 (2018) 1774–1781.
[88] M.C. Arenas, E. Andablo, V.M. Castaño, Synthesis of conducting polyaniline nanofibers from single and binary dopant agents, J. Nanosci. Nanotechnol. 10 (2010) 549–554.
[89] C. Merlini, G.M.O. Barra, D.P. Schmitz, S.D.A.S. Ramôa, A. Silveira, T.M. Araujo, A. Pegoretti, Polyaniline-coated coconut fibers: structure, properties and their use as conductive additives in matrix of polyurethane derived from castor oil, Polym. Test. 38 (2014) 18–25.
[91] U. Male, P. Srinivasan, B.S. Singu, Incorporation of polyaniline nanofibres on graphene oxide by interfacial polymerization pathway for supercapacitor, Int. Nano Lett. 5 (2015) 231–240.
[93] S. Tanwar, J. Ho, Green synthesis of novel polyaniline nanofibers: application in pH sensing, Molecules 20 (2015) 18585–18596.
[94] H. Gao, Z. Song, W. Zhang, X. Yang, X. Wang, D. Wang, Synthesis of highly effective absorbents with waste quenching blast furnace slag to remove Methyl Orange from aqueous solution, J. Environ. Sci. (China). 53 (2017) 68–77.
[95] R. Huang, Q. Liu, J. Huo, B. Yang, Adsorption of methyl orange onto protonated cross-linked chitosan, Arab, J. Chem. 10 (2017) 24–32.
[96] S. Rattanapan, J. Srikram, P. Kongsune, Adsorption of methyl orange on coffee grounds activated carbon, Energy Proc. 138 (2017) 949–954.

[97] C. Umpuch, S. Sakaew, Removal of methyl orange from synthetic wastewater onto chitosan-coated-montmorillonite Clay in Fixed-Beds 6, 2012, pp. 175–180.
[98] A.A. Alghamdi, A.B. Al-Odayni, W.S. Saeed, M.S. Almutairi, F.A. Alharthi, T. Aouak, A. Al-Kahtani, Adsorption of azo dye methyl orange from aqueous solutions using alkali-activated polypyrrole-based graphene oxide, Molecules 24 (2019).
[99] M. Bhaumik, R. McCrindle, A. Maity, Efficient removal of Congo red from aqueous solutions by adsorption onto interconnected polypyrrole-polyaniline nanofibres, Chem. Eng. J. 228 (2013) 506–515.
[100] Y. Long, D. Lei, J. Ni, Z. Ren, C. Chen, H. Xu, Packed bed column studies on lead(II) removal from industrial wastewater by modified Agaricus bisporus, Bioresour. Technol. 152 (2014) 457–463.
[101] A. Negrea, L. Lupa, M. Ciopec, P. Negrea, Experimental and modelling studies on as (III) removal from aqueous medium on fixed bed Column 56, 2011, pp. 89–93.
[102] V.C. Taty-Costodes, H. Fauduet, C. Porte, Y.S. Ho, Removal of lead (II) ions from synthetic and real effluents using immobilized Pinus sylvestris sawdust: adsorption on a fixed-bed column, J. Hazard Mater. 123 (2005) 135–144.
[103] J.O. Kittinya, M.S. Onyango, A. Ochieng, Fixed-bed column breakthrough analysis for the removal of reactive red 2 dye from aqueous solution using zeolite-polyaniline nanocomposite, in: Int. Conf. Chem. Eng. Adv. Comput. Technol. (ICCEACT'2014), Nov 24-25, 2014, Pretoria, SOuth Africa, 2014, pp. 2–6.
[104] G. Murithi, K. Thiong, K.S. Warui, W. Muthengia, Fixed column study for the removal of zinc (II) ions from waste water by bone char rice husks ash and water hyacinth composite-mixture, Int. J. Sci. Res. 5 (2016) 708–714.
[105] V. Janaki, B.T. Oh, K. Shanthi, K.J. Lee, A.K. Ramasamy, S. Kamala-Kannan, Polyaniline/chitosan composite: an eco-friendly polymer for enhanced removal of dyes from aqueous solution, Synth. Met. 162 (2012) 974–980.
[106] R.X. Wang, L.F. Huang, X.Y. Tian, Understanding the protonation of polyaniline and polyaniline-graphene interaction, J. Phys. Chem. C 116 (2012) 13120–13126.
[107] J. Stejskal, P. Kratochvíl, A.D. Jenkins, Polyaniline: forms and formation, Collect. Czech Chem. Commun. 60 (1995) 1747–1755.